

Scalable collective Lamb shift of a 1D superconducting qubit array in front of a mirror

Kuan-Ting Lin¹, Ting Hsu¹, Chen-Yu Lee¹, Io-Chun Hoi², and Guin-Dar Lin¹

¹*Center for Quantum Science and Engineering, Department of Physics,
National Taiwan University, Taipei 10617, Taiwan and*

²*Center for Quantum Technology and Department of Physics,
National Tsing Hua University, Hsinchu 30013, Taiwan*

We theoretically investigate resonant dipole-dipole interaction (RDDI) between artificial atoms in a 1D geometry, implemented by N transmon qubits coupled through a transmission line. Similarly to the atomic cases, RDDI comes from exchange of virtual photons of the unexcited modes, and causes the so-called collective Lamb shift (CLS). To probe the shift, we effectively set one end of the transmission line as a mirror, and examine the reflection spectrum of the probe field from the other end. Our calculation shows that when a qubit is placed at the node of the standing wave formed by the incident and reflected waves, even though it is considered to be decoupled from the field, it results in large energy splitting in the spectral profile of a resonant qubit located elsewhere. This directly signals the interplay of virtual photon processes and explicitly demonstrates the CLS. We further derive a master equation to describe the system, which can take into account mismatch of participating qubits and dephasing effects. Our calculation also demonstrates the superradiant and subradiant nature of the atomic states, and how the CLS scales when more qubits are involved.

I. INTRODUCTION

One of the intriguing phenomena of quantum electrodynamics is the emergence of the Lamb shift, which was first discovered by Lamb in 1947 [1], corresponding to the energy difference between $2S_{1/2}$ and $2P_{1/2}$ levels of a hydrogen atom. The understanding of such a shift opened up a new chapter of physics now known as quantum field theory, bringing in a concept that quantum vacuum must be treated as a zero-point state of numerous harmonic oscillators (photon modes), and quantum fluctuations allow both real and virtual processes to have physical effects. This perspective of quantum vacuum also plays an essential role in various scenarios such as spontaneous decay emission, squeezed vacuum states [2, 3], and the Casimir effect [4–6]. Recently, resonant dipole-dipole interaction (RDDI) mediated via exchange of virtual photons between multiple atoms has become one of the most interesting topics in different contexts [7–12]. Such RDDI results in the collective version of Lamb shift, sometimes also termed the cooperative Lamb shift (CLS) due to its close connection to cooperative phenomena such as super- and subradiance [13–15]. For past few years, CLS regarding atomic systems have been experimentally demonstrated and studied in atomic clouds [16, 17], in nano-layer gases [18, 19], ensembles of embedded nuclei [20], and trapped ions [21]. Main challenges of observing CLS in atomic systems originate from vacuum mediated coupling weakened very fast as separation increases in 3D space. In order to probe the shift, ideally atoms must be placed at a distance comparable to the transition wavelength, or inside cavities or waveguides where field can be confined or directed, thus enhancing the interaction strength. Based on such consideration, it is suggested that the circuit quantum electrodynamical (circuit QED, or cQED) systems are a perfect testbed for observing cooperative phenomena.

Circuit QED systems deal with superconducting arti-

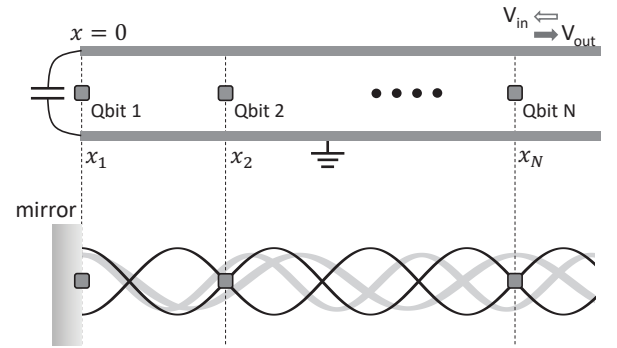


FIG. 1. Architecture of the 1D array of transmon qubits coupled through a microwave waveguide, whose one end is terminated by a large capacitor at $x = 0$, effectively serving as an antinode mirror. The probe field is fed from the other end of the waveguide, coherently superposes with the reflected field, forming a standing wave. When other qubits are placed at the nodes, they do not directly interact with probe photons. However, the qubits can still couple to other vacuum modes of continuous spectrum, mediating the RDDI only through virtual processes.

ficial atoms coupled through 1D microwave waveguides. They are relatively more easily fabricated to achieve the strong coupling or the superradiant regime compared to the atomic counterpart [22], and have been used extensively to study the Tavis-Cummings model [23], dipole-dipole coupling [24], photon-ensemble interaction, super- and subradiance [25–29], and quantum information oriented applications [30, 31]. Up to present, the observation of CLS in cQED systems is still scarce except for [26], where two qubits are both pumped in an open waveguide, resulting in collective decay linewidth larger than the shift, seriously degrading the visibility of CLS. We here study the emergence of CLS when a series of transmon qubits are arranged in front of a mirror, and probed

for the reflection spectrum. In order to identify RDDI that is exclusively from mediation of virtual photons, we put one qubit at an antinode while others at nodes with respect to their transition wavelength as shown in Fig. 1. Intuitively speaking, since these qubits at nodes do not directly interact with the probing field, they have no effect on the antinode qubit's spectral profile through real photon exchange. This is however not the entire story because one neglects contributions from the whole range of vacuum modes, which, except for the resonant one, are not physically excited but in fact responsible for RDDI. The advantage of insertion of a mirror is to introduce destructive interference that suppresses the collective decay linewidth, hence improving the visibility of the CLS.

This paper is organized as follows: Sec. II presents a cQED system of a half-infinite waveguide, and derives the model for RDDI associated with it. Sec. III mainly discusses two-qubit cases, focusing on the superradiant condition and emergence of CLS. We calculate the reflection spectrum, commonly measured in current experiments [32–34], showing the observable CLS splitting in the profile. We also study the dephasing and power broadening effects as well as level anharmonicity for real transmon artificial atoms. Sec. IV discusses multi-qubit cases, demonstrating the scaling law for the CLS and number of qubits. To explain this we present an effective reduced scheme. Finally we conclude this work in Sec. V.

II. MODEL

A. Dipole-dipole interaction and master equation

We consider a linear chain of N transmon qubits coupled to a common 1D waveguide whose one end is terminated by a very large capacitor. This amounts to set the end as an antinode mirror regarding the standing waves in such an architecture. Different from a discrete spectrum in a cavity case with two mirrors, our system allows continuum of the photon modes. The Hamiltonian describing this system can be written as $H = H_S + H_B + H_{int}$ [32, 35–37] with the atomic part $H_S = \sum_i \hbar \omega_i \sigma_i^+ \sigma_i^-$, the field part $H_B = \int_0^\infty \hbar \omega a_\omega^\dagger a_\omega d\omega$, and the interaction under the rotating wave approximation

$$H_{int} = i \sum_i \int_0^\infty d\omega \hbar g_i(\omega) \cos(k_\omega x_i) a_\omega \sigma_i^+ + H.c.. \quad (1)$$

Here, ω_i denotes the transition frequency between the excited state $|e\rangle_i$ and the ground one $|g\rangle_i$ of the i th qubit located at x_i , and $\sigma_i^+ = |e\rangle_i \langle g|$ and $\sigma_i^- = |g\rangle_i \langle e|$ represent its raising and lowering operators, respectively. The operator a_ω^\dagger (a_ω) creates (annihilates) a photon of frequency ω , whose mode function is of the form $\sim \cos k_\omega x$ due to presence of the antinode mirror at $x = 0$. The wavenumber $k_\omega = \omega/v$ with v the speed of light in the waveguide.

Note that a_ω^+ and a_ω satisfy the commutation relation $[a_\omega^+, a_\omega] = \delta(\omega - \omega')$. Following the standard procedure to trace out the photonic degrees of freedom [38] and applying the Born-Markov approximation, we arrive at the master equation

$$\begin{aligned} \frac{d\rho}{dt} = & i \sum_i \delta_i [\sigma_i^+ \sigma_i^-, \rho] \\ & - i \sum_{ij} (\Delta_{ij}^+ - i\gamma_{ij}^-) [\sigma_i^+ \sigma_j^-, \rho] \\ & + i \sum_i \Omega_p^i \cos(k_p x_i) [\sigma_i^+ + \sigma_i^-, \rho] \\ & + \sum_{ij} (\gamma_{ij}^+ + i\Delta_{ij}^-) \mathcal{L}_{ij}[\rho] \\ & + \sum_i \gamma_i^\phi \mathcal{L}_i^\phi[\rho]. \end{aligned} \quad (2)$$

In this master equation, we have explicitly included a continuous-wave probe field incident from the other end of the waveguide with a detuning $\delta_i = \omega_p - \omega_i$, the associated Rabi frequency Ω_p^i seen by the i th qubit, and a wavenumber $k_p = \omega_p/v$. The superoperator $\mathcal{L}_{ij}[\rho] \equiv 2\sigma_j^- \rho \sigma_j^+ - \sigma_i^+ \sigma_j^- \rho - \rho \sigma_i^+ \sigma_j^-$ deals with self and cooperative dissipative processes. And $\mathcal{L}_i^\phi[\rho] \equiv 2\sigma_i^{ee} \rho \sigma_i^{ee} - \sigma_i^{ee} \rho - \rho \sigma_i^{ee}$ with $\sigma_i^{ee} = |e\rangle_i \langle e|$ is added by hand to account for individual pure dephasing characterized by γ_i^ϕ . The dipole-dipole interaction, obtained by summing all contributions from the photon mode continuum, is now contained in $\gamma_{ij}^\pm = (\gamma_{ij} \pm \gamma_{ji})/2$ and $\Delta_{ij}^\pm = (\Delta_{ij} \pm \Delta_{ji})/2$ with

$$\gamma_{ij} = \frac{\gamma_{ij}^0}{2} [\cos k_j(x_i + x_j) + \cos k_j |x_i - x_j|] \quad (3)$$

$$\Delta_{ij} = \frac{\gamma_{ij}^0}{2} [\sin k_j(x_i + x_j) + \sin k_j |x_i - x_j|], \quad (4)$$

where $\gamma_{ij}^0 \equiv \sqrt{\gamma_i(\omega_j)\gamma_j(\omega_j)}$ with the bare decay rate $\gamma_i = \pi g_i^2(\omega_j)$ evaluated at the j th qubit's transition frequency ω_j (see Appendix A for details).

Here are a few remarks regarding the forms of Eqs. (3) and (4). First, for an open waveguide without a mirror, it can be proven that the dipole-dipole interaction between the i th and j th qubits depends only on the relative distance $|x_i - x_j|$ [22]. The mirror effectively places image atoms on the other side of the mirror. Therefore qubit i does not only see the real qubit j at a distance $|x_i - x_j|$ but also the image one at distance $(x_i + x_j)$. Secondly, these rates and shifts are related through the Kramers-Kronig (KK) relations

$$\gamma_{ij} = \frac{1}{\pi} \int \frac{\Delta_{ij}(\omega')}{\omega - \omega'} d\omega' \quad (5)$$

$$\Delta_{ij} = -\frac{1}{\pi} \int \frac{\gamma_{ij}(\omega')}{\omega - \omega'} d\omega'. \quad (6)$$

Note that, in general, γ_{ij}^\pm and Δ_{ij}^\pm are non-zero with non-identical qubits, leading to non-Lindblad behavior

[39]. For identical qubits where the sub-indices are interchangeable, γ_{ij}^- and Δ_{ij}^- vanish and hence the master equation retains the Lindblad form; Δ_{ij} then directly contributes to the CLS.

B. Scattering and Reflection

In order to probe the CLS configuration, we manage to feed the probe signal from and acquire its reflection spectrum on the open end. As measured in many experiments [32, 33, 36, 40], the reflection coefficient is obtained by

$$r(x, t) \equiv |V_{out}(x, t)/V_{in}(x, t)|, \quad (7)$$

where the output signal $V_{out}(x, t) = V_{in}(x, t) + V_{sc}(x, t)$ with the input voltage V_{in} and scattered one V_{sc} . The input signal is assumed to be of the form

$$V_{in}(x, t) = V_0 e^{ik_p x} \quad (8)$$

viewed from the rotating frame of the probe frequency, where V_0 is the amplitude of the input voltage with its corresponding wave number k_p . The scattered voltage can be calculated from the flux [36, 41]

$$\Phi(x, t) = \sqrt{\frac{\hbar Z_0}{\pi}} \int \frac{d\omega}{\sqrt{\omega}} \cos k_\omega x (a_\omega + a_\omega^\dagger) \quad (9)$$

with the characteristic impedance Z_0 . Then the scattered signal is obtained by differentiating the positive frequency part $V_{sc} = \partial \Phi^{out} / \partial t$ for the outgoing wave. In the probe-frequency frame,

$$V_{sc}(x, t) = -i \sqrt{\frac{\hbar Z_0}{4\pi}} \int_0^\infty \sqrt{\omega} \tilde{a}_\omega(t) e^{ik_\omega x - i(\omega - \omega_p)t} d\omega. \quad (10)$$

Here we have used the fact that the field operator can be expressed in terms of the slowly-varying amplitude $a_\omega(t) = \tilde{a}_\omega(t) e^{-i\omega t}$ and $\dot{\tilde{a}}_\omega \approx 0$. Through the standard procedures, as summarized in Appendix A, the photonic operator is related to the atomic one [42, 43]

$$\tilde{a}_\omega(t) = - \sum_{i=1}^N g_i(\omega) \int_0^t \tilde{\sigma}_i^-(t') e^{i(\omega - \omega_i)t'} dt', \quad (11)$$

where the atomic operator is also assumed of the form $\sigma_i^-(t) = \tilde{\sigma}_i^-(t) e^{-i\omega_i t}$. Substituting Eq. (11) into Eq. (10), and using Eqs. (7) and (8), we then have the scattered signal and the reflection coefficient, respectively,

$$V_{sc} = i \sum_{i=1}^N \sqrt{\hbar \pi Z_0 \omega_i} g_i(\omega_i) \tilde{\sigma}_i^-, \quad (12)$$

$$r = \left| 1 + i \sum_{i=1}^N \sqrt{\hbar \pi Z_0 \omega_i} g_i(\omega_i) \cos k_p x_i \langle \sigma_i^- \rangle / V_0 \right|. \quad (13)$$

The photon-atom coupling strength for transmon qubits is given by

$$g_i(\omega) = e\beta_i \left(\frac{E_J^{(i)}}{8E_C^{(i)}} \right)^{1/4} \sqrt{\frac{2Z_0\omega}{\pi\hbar}}, \quad (14)$$

where e is the electron charge; Z_0 is the characteristic impedance of the transmission line; $\beta_i = C_C^i/C_T^i$ is the ratio between the capacitor C_C^i of the transmission line and the total capacitor C_T^i ; $E_J^{(i)}$ and $E_C^{(i)}$ are the Josephson energy and the charging energy, respectively, of the i th qubit [35, 44, 45]. Note that the input voltage V_0 is viewed right outside the outmost qubit (the N th one), and is connected to the Rabi frequency via

$$V_0 = \frac{\Omega_p^N}{2g_N(\omega)} \sqrt{\frac{\hbar Z_0 \omega}{\pi}}. \quad (15)$$

By expressing V_0 in terms of Ω_p , we finally obtain the reflection coefficient

$$r = \left| 1 + i \sum_{i=1}^N \frac{2\eta_{Ni}\gamma_i}{\Omega_p^N} \cos k_p x_i \langle \sigma_i^- \rangle \right|, \quad (16)$$

with $\eta_{Ni} = (E_J^{(N)} E_C^{(i)} / E_J^{(i)} E_C^{(N)})^{1/4} \beta_N / \beta_i$. The atomic variables $\langle \sigma_i^- \rangle$ needs to be solved by evaluating the master equation (2), which can be done numerically, or analytically only under the weak field approximation for the steady state. We will discuss the results in the following sections.

III. SUPERRADIANCE AND COLLECTIVE LAMB SHIFT FOR TWO-ATOM CASES

A. Reflection spectrum

We start with discussion for the simplest case of two identical qubits, who share the same frequency and bare decay rate, $\omega_1 = \omega_2 \equiv \omega_0$ and $\gamma_{12}^0 = \gamma_{21}^0 \equiv \gamma_0$, respectively. In this case, $\Delta_{12}^- = \gamma_{12}^- = 0$, $\Delta_{12}^+ = \Delta_{12}(x_1, x_2)$, $\gamma_{12}^+ = \gamma_{12}(x_1, x_2)$, and $\eta_{21} = 1$. Fig. 2 shows the self and cooperative decay rates and energy shifts according to Eqs. (3) and (4). Here, we set $x_1 = 0$, i.e., the 1st qubit is placed at the antinode mirror, and vary the position x_2 of the 2nd one. Since γ_{12} and Δ_{12} are periodic functions of x_2 , we will not lose generality if only discuss $1 \leq x_2/\lambda \leq 2$ with $\lambda = 2\pi v/\omega_0$. For decay rates shown in Fig. 2 (a), it can be observed that the spontaneous ones are proportional to the strength of the local field: γ_{11} remains at the maximal value due to the antinode at $x_1 = 0$, and γ_{22} oscillates harmonically following the intensity of the standing wave of resonant (of period $\lambda/2$) as x_2 increases. The mutual decay rates γ_{12} also oscillates in space but of period λ . Note that γ_{12} changes sign every half a wavelength, suggesting the interchange

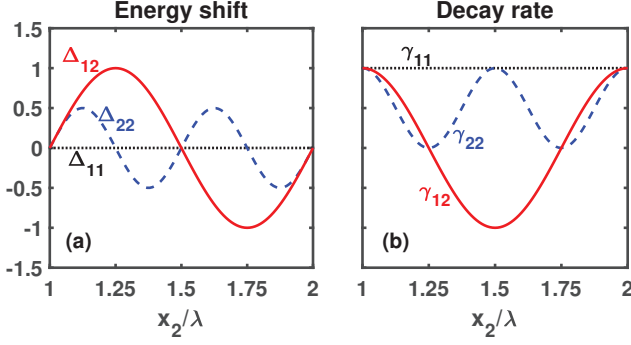


FIG. 2. Energy shifts and decay rates (in units of γ_0) of the two-qubit system for varied x_2 . Δ_{ii} and γ_{ii} represent the single-atom energy shift and spontaneous decay rate, respectively, for the i th qubit. Δ_{12} and γ_{12} correspond to the exchange interaction and the mutual decay rate, respectively. Note that $x/\lambda = 1, 1.5, 2, \dots$ correspond to nodes of the resonant field while $x/\lambda = 1.25, 1.75, \dots$ correspond to antinodes.

of the super- and subradiant nature between the symmetric and anti-symmetric states. Further, in Fig. 2 (b) we find that the energy shift Δ_{22} for the 2nd qubit also displays oscillatory features, following the same period of its KK counterpart γ_{22} . But the amount of shift vanishes at the locations of both nodes and antinodes ($\Delta_{11} = 0$ due to x_1 fixed at the antinode). On the other hand, the mutual coupling Δ_{12} deals with the exchange interaction between two qubits. It is noticeable that although Δ_{12} , as the KK counterpart of γ_{12} , vanishes at antinodes, it reaches the maximum magnitude at nodes. The nonzero coupling mixes the symmetric and anti-symmetric states, and introduces a finite CLS, which, we will show in the following, is visible in the reflection spectrum.

The reflection amplitude coefficient Eq. (16) can be directly computed through solving the steady state from the master Eq. (2) numerically. Fig. 3(a) maps out the reflection spectrum from $x_2/\lambda = 1$ (antinode) to $x_2/\lambda = 1.5$ (next antinode). To understand the spectrum, it is instructional to perform analysis under certain approximation and circumstances. We here only briefly summarize the method we use and the results for two qubits for (i) $x_2/\lambda = 1$ (antinode), and (ii) $x_2/\lambda = 1.25$ (node) with $x_1 = 0$ in both cases. Note that Eq. (16) can be reduced to the standard Lindblad form [7, 46–49], and recast into the Dicke representation. For $x_2/\lambda = 1$, we go to the non-Hermitian effective Hamiltonian:

$$\begin{aligned}
 H_{eff} = & -\hbar\delta(D_s^+ D_s^- + D_a^+ D_a^-) \\
 & -\hbar\sqrt{2}\Omega_p(D_s^+ + D_s^-) \\
 & -i\hbar\Gamma D_s^+ D_s^- - i\hbar\left(\frac{\gamma_1^\phi + \gamma_2^\phi}{2}\right) D_a^+ D_a^-, \quad (17) \\
 & -i\hbar\left(\frac{\gamma_1^\phi - \gamma_2^\phi}{2}\right) (D_s^+ D_a^- - D_a^+ D_s^-)
 \end{aligned}$$

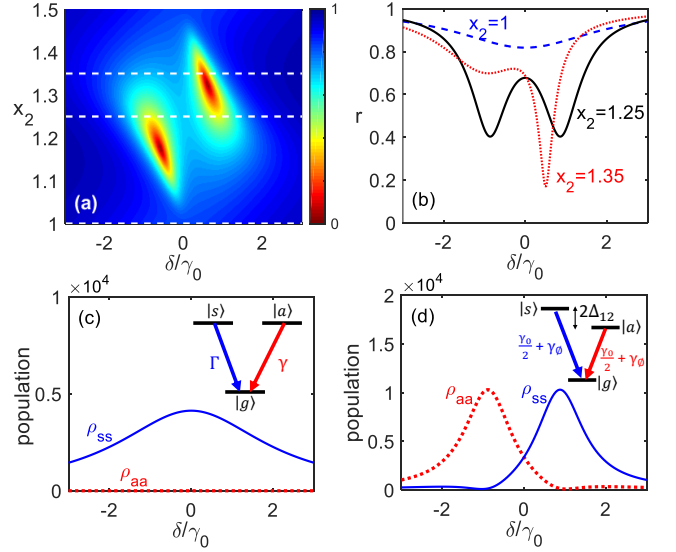


FIG. 3. (a) Reflection spectrum for various x_2 in units of λ with $x_1 = 0$. (b) The profiles corresponding to three white dashed line cuts in (a). For $x_2/\lambda = 1$ (antinode), the spectral profile presents a single wide dip, signaling the superradiant nature. For $x_2/\lambda = 1.25$ (node), the symmetric and antisymmetric states are split due to the CLS so that two dips merge corresponding to two resonant conditions. For x_2 away from the antinode, two dips move to the side of red detuning with the left one rising and finally fading out, and the right one moving toward the middle, and finally becoming superradiant as x_2 reaches the next antinode. (c) Population as a function of detuning in the symmetric (ρ_{ss}) and antisymmetric (ρ_{aa}) states for $x_2/\lambda = 1$. (d) Similar to (c) but for $x_2/\lambda = 1.25$. Note that for $1.5 \leq x_2/\lambda \leq 2$, these curves are similar but with the roles of the symmetric and antisymmetric states are switched. (Other parameters: $\gamma_\phi = 0.2\gamma_0$ and $\Omega_p = 0.01\gamma_0$.)

where the collective symmetric and anti-symmetric operators are defined by $D_s^\pm = \frac{1}{\sqrt{2}}(\sigma_1^\pm + \sigma_2^\pm)$ and $D_a^\pm = \frac{1}{\sqrt{2}}(\sigma_1^\pm - \sigma_2^\pm)$, respectively, with the superradiant decay rate $\Gamma = 2\gamma_0 + \frac{\gamma_1^\phi + \gamma_2^\phi}{2}$. Here, assuming the dephasing rate $\gamma_1^\phi = \gamma_2^\phi = \gamma_\phi$ shared by the qubits, we write the two-qubit state $|\psi\rangle = c_g|g\rangle + c_s|s\rangle + c_a|a\rangle + c_e|e\rangle$, where $|g\rangle \equiv |gg\rangle$, $|e\rangle \equiv |ee\rangle$, $|s\rangle = (|ge\rangle + |eg\rangle)/\sqrt{2}$, and $|a\rangle = (|ge\rangle - |eg\rangle)/\sqrt{2}$. In the weak-field approximation, $\Omega_p \ll \gamma_0$, $c_g \approx 1$, we thus omit the higher order terms $\mathcal{O}(\Omega_p^2)$, and then have $D_s^+ \approx |s\rangle\langle g|$ and $D_a^+ \approx |a\rangle\langle g|$. The steady-state solution to the Schrodinger's equation $i\hbar\frac{d}{dt}|\psi\rangle = H_{eff}|\psi\rangle$ is

$$c_s = \frac{\sqrt{2}i\Omega_p(\gamma_\phi - i\delta)}{2\gamma_0\gamma_\phi + \gamma_\phi^2 - \delta^2 - 2i\delta(\gamma_0 + \gamma_\phi)} \quad (18)$$

$$c_a = 0. \quad (19)$$

Plugging c_s and c_a into Eq. (16) using $\langle\sigma_{1,2}^-\rangle = \frac{1}{\sqrt{2}}(c_s \pm c_a)$, we can obtain

$$r = \left| 1 - \frac{4\gamma_0(\gamma_\phi - i\delta)}{2\gamma_0\gamma_\phi + \gamma_\phi^2 - \delta^2 - 2i\delta(\gamma_0 + \gamma_\phi)} \right|, \quad (20)$$

which, when γ_ϕ is negligible, approaches $\left| 1 - \frac{4\gamma_0\gamma_\phi}{\delta^2 + 4\gamma_0^2} \right|^{1/2}$ forming a central dip of width $2\gamma_0$. This corresponds to the Dicke superradiant condition that the linewidth is broadened by a factor of 2 for two qubits. Also, we can see that only the symmetric state $|s\rangle$ is occupied with population $\rho_{ss} = |c_s|^2$ because the anti-symmetric state is decoupled. Note that when $x_2/\lambda = 1.5$, the roles of the symmetric and antisymmetric states are switched because $\gamma_{12} = -\gamma_0$ and $\sigma_1^\pm + (-1)^{2x_2/\lambda}\sigma_2^\pm \rightarrow \sqrt{2}D_a^\pm$, and also $\Gamma \rightarrow \gamma_\phi$ and $\gamma \rightarrow 2\gamma_0 + \gamma_\phi$ in Eq. (17).

For $x_2 = 1.25\lambda$, the Hamiltonian then becomes

$$\begin{aligned} H_{eff} = & \hbar(-\delta + \Delta_{12})D_s^+D_s^- \\ & + \hbar(-\delta - \Delta_{12})D_a^+D_a^- \\ & - \frac{\hbar\Omega_p}{\sqrt{2}}(D_s^+ + D_s^- + D_a^+ + D_a^-) \\ & - i\hbar\gamma^+(D_s^+D_s^- + D_a^+D_a^-) \\ & - i\hbar\gamma^-(D_s^+D_a^- - D_a^+D_s^-) \end{aligned} \quad (21)$$

with

$$\gamma^\pm = \frac{\gamma_0 + \gamma_{\phi_1} \pm \gamma_{\phi_2}}{2}. \quad (22)$$

Similar analysis leads to the solution

$$c_s = \frac{\frac{i\Omega_p}{\sqrt{2}}[\gamma_2^\phi - i(\delta + \Delta_{12})]}{(\gamma_0 + \gamma_1^\phi)\gamma_2^\phi - (\delta^2 - \Delta_{12}^2) - 2i\delta\gamma^+} \quad (23)$$

$$c_a = \frac{\frac{i\Omega_p}{\sqrt{2}}[\gamma_2^\phi - i(\delta - \Delta_{12})]}{(\gamma_0 + \gamma_1^\phi)\gamma_2^\phi - (\delta^2 - \Delta_{12}^2) - 2i\delta\gamma^+} \quad (24)$$

and hence

$$r = \left| 1 - \frac{2\gamma_0(\gamma_2^\phi - i\delta)}{(\gamma_0 + \gamma_1^\phi)\gamma_2^\phi - (\delta^2 - \Delta_{12}^2) - 2i\delta\gamma^+} \right|. \quad (25)$$

For small γ_2^ϕ , two dips correspond to $\delta \rightarrow \delta_\pm$ with

$$\delta_\pm \approx \pm\Delta_{12} \left[1 - \frac{\gamma_0^2 - \gamma_1^{\phi 2}}{4\Delta_{12}^2} \frac{\gamma_2^\phi}{\gamma_1^\phi} \right] \rightarrow \pm\Delta_{12} \quad (26)$$

as $\gamma_2^\phi \rightarrow 0$. This is consistent with our previous argument that Δ_{12} contributes to a coupling between $|s\rangle$ and $|a\rangle$ and splits the two states. Therefore, the CLS directly results in the spectral splitting $\delta_{split} \equiv 2|\delta_\pm| \approx 2\Delta_{12}$ directly evident in the reflection profile. Finally, note that at $\delta = -\Delta_{12}$, $\rho_{ss} \approx \frac{|\Omega_p|^2\gamma_2^{\phi 2}}{2\Delta_{12}^2\gamma_0^2} \rightarrow 0$ as $\gamma_2^\phi \rightarrow 0$, implying that all the excitation is populated on state $|a\rangle$. Conversely, at $\delta = +\Delta_{12}$, only state $|s\rangle$ is populated. In the case of $x_2/\lambda = 1.75$, the roles of the symmetric and antisymmetric states are switched due to the same argument in the case of $x_2/\lambda = 1.5$ discussed previously.

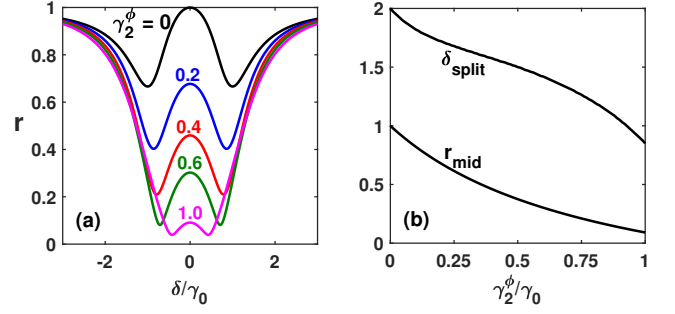


FIG. 4. (a) Reflection spectrum for various dephasing rates of the 2nd qubit at $x_2/\lambda = 1.25$. Here we set $\gamma_1^\phi = 0.2\gamma_0$ and $\Omega_p = 0.01\gamma_0$. (b) Spectral splitting δ_{split} in units of γ_0 and the height of the central maximum r_{mid} as monotonically descending functions of the 2nd qubit's dephasing rate γ_2^ϕ .

B. Dephasing

We now examine the effect of dephasing on the splitting feature. Intuitively speaking, dephasing usually introduces broadening that degrades the quantum effects from being observed. In our case, however, when we take $\gamma_1^\phi = \gamma_2^\phi = 0$, Eq. (25) gives $r = 1$ constant reflection profile for any finite detuning δ . Therefore the splitting information will be hidden. In fact, we need $\gamma_1^\phi > 0$ in order to view splitting as a trace of CLS from the reflection spectrum. We have shown in Eq. (26) that $\delta_\pm \rightarrow \pm\Delta_{12}$ as $\gamma_2^\phi \rightarrow 0$ for any $\gamma_1^\phi > 0$. When $\gamma_2^\phi > 0$, we find that the mismatch between δ_{split} and $2\Delta_{12}$ has a leading-order term proportional to $\gamma_2^\phi/\gamma_1^\phi$, which suggests that $\delta_\pm \rightarrow \pm\Delta_{12}$ as long as $\gamma_2^\phi/\gamma_1^\phi$ is small.

Figure 4 shows our numerical calculation when $\gamma_1^\phi = 0.2\gamma_0$ is fixed, corresponding to a typical experimental realization. When γ_2^ϕ increases from zero, we find δ_{split} decreases monotonically from $2\Delta_{12}$. Another interesting feature regarding visibility of CLS is the central maximum $r_{mid} \equiv r(\delta = 0)$, which is also lowered with increasing γ_2^ϕ according to

$$r_{mid} = 1 - \frac{2\gamma_{11}\gamma_2^\phi}{(\gamma_{11} + \gamma_1^\phi)\gamma_2^\phi + \Delta_{12}^2}. \quad (27)$$

In real experiments [34], this maximum is always smaller than unity, reflecting the presence of dephasing mechanisms on the 2nd qubit. We find that r_{mid} is dominantly determined by γ_2^ϕ and insensitive to γ_1^ϕ according to Eq. (27). Thus r_{mid} provides a very good indication to be used to extract γ_2^ϕ by neglecting γ_1^ϕ . The ratio of γ_2^ϕ thus obtained to the actual value is $\Delta_{12}^2/(\Delta_{12}^2 + \gamma_1^\phi\gamma_2^\phi)$. Therefore, for $\gamma_1^\phi, \gamma_2^\phi \sim 0.5\gamma_0$, the estimated value of γ_2^ϕ is 20% less than the actual one; for $\gamma_1^\phi, \gamma_2^\phi \sim 0.2\gamma_0$ as in a typical experiment, it becomes only 4% less.

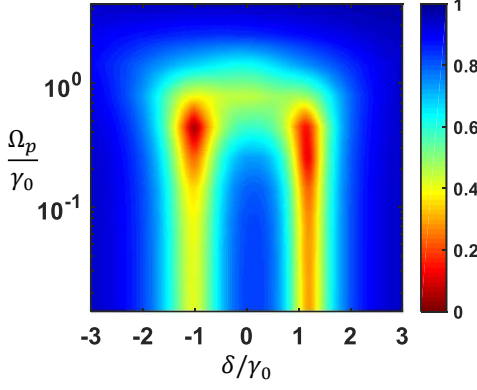


FIG. 5. Power broadening of the reflection spectrum of one qubit located at $x_1 = 0$ and one at $x_2 = 1.755\lambda$, slightly off the node of the standing wave. See text for other parameters.

C. Power broadening

In preceding discussion, we have focused on the weak field limit on two identical qubits with one located at the anti-node and the other at the node perfectly. In this section, we discuss a more realistic case with parameters given in the experiment [34]. For strong probing, the effective-Hamiltonian approach breaks down at some point due to significant population in the upper level. To account for the associated effect, we generalize our model to multi-level atoms (see Appendix B), where the anharmonicity of transmon qubits is explicitly considered, and numerically solve the master equation Eq. (A.10). A typical power dependent reflection spectrum is shown in Fig. 5. Here, we have used $\omega_1 = 2\pi \times 4.755$ GHz and $\omega_2 = 2\pi \times 4.759$ GHz for two atoms at $x_1 = 0$ and $x_2 = 1.755\lambda$, respectively, where $\lambda = 2\pi v/\omega_2$ with wavespeed $v = 0.8948 \times 10^8$ m/s. Further, $\gamma_{11} \approx \gamma_{12}^0 \approx \gamma_{21}^0 \approx \gamma_0 = 2\pi \times 17.2$ MHz, $\gamma_{22} \approx 2\pi \times 0.02$ MHz, the anharmonicity is $2\pi \times 406$ MHz and $2\pi \times 324$ MHz for the 1st and 2nd atoms, respectively. The dephasing rates are $0.17\gamma_0$ ($0.28\gamma_0$) and $0.13\gamma_0$ ($0.25\gamma_0$) for the lower (upper) level transition of the 1st and 2nd atoms, respectively.

For weak probing $\Omega_p \lesssim 0.1\gamma_0$, the spectrum profiles remain independent of the probe power, reflecting the fact that the CLS originates from vacuum modes rather than the real photon field. As Ω_p increases, we see clear power broadening of the two dips due to significant population in the second level. Note that the spectral profile being slightly shifted to the right is because of frequency mismatch of the two qubits. And the obvious asymmetry of the profile is owing to the fact that the 2nd qubit is not perfectly placed at the node and contributes to the scattered signal. Though our model explicitly considers the third level, our numerical results suggest that its role is almost negligible as long as the anharmonicity is greater than $5\gamma_0 \approx 2\pi \times 87$ MHz. For $\Omega_p \gtrsim 2\gamma_0$, the system gets

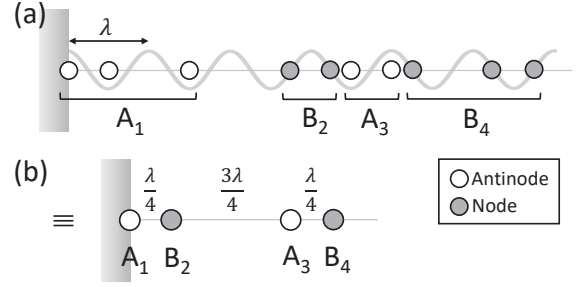


FIG. 6. (a) Array of qubits located at either nodes and antinodes. (b) Equivalent reduced scheme of “giant atoms” arranged at antinodes and nodes alternatively.

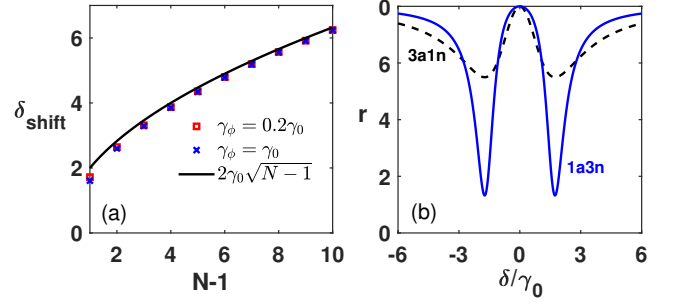


FIG. 7. (a) CLS splitting $\delta_{split} \approx 2\gamma_0\sqrt{N-1}$ for an qubit array of one at the mirror ($x_1 = 0$) and $N-1$ ones at nodes. Small deviations can be observed with finite dephasing rate γ_ϕ for all the qubits. (b) Spectral profiles for three antinode qubits plus one node qubit (3a1n) and one antinode qubit plus three node ones (1a3n).

saturated and attains unity reflection.

IV. MULTI-ATOM CASES

We now consider multi-atom cases with $N \geq 3$. Although the system’s dynamics can be fully determined by evolving the master equation (2) for arbitrary arrangements of qubits, we here focus on configurations with identical qubits either at antinodes or nodes as shown in Fig. 6 (a). For analysis, we first take those qubits at antinodes/nodes in a row as a group. By doing so, the system now consists of antinode groups (A_j) and node ones (B_j) placed in alternative order, i.e., $A_1 B_2 A_3 B_4 \dots$. For each antinode group, we define the collective operator as $S_j^\pm \equiv \sum_{i \in A_j} (-1)^{2x_i/\lambda} \sigma_i^\pm$, and for each node one $S_j^\pm = \sum_{i \in B_j} (-1)^{2x_i/\lambda - 0.5} \sigma_i^\pm$. Under the weak field approximation with only single excitation allowed, $S_j^+ \approx |s\rangle_{A_j} \langle g|^{\otimes n_j}$ with $|s\rangle$ a superradiant state. For instance, for the case $(x_1, x_2, x_3) = (0, 1, 1.5)\lambda$, $S^+ = \sigma_1^+ + \sigma_2^+ - \sigma_3^+$, the superradiant state is given by $|s\rangle = \frac{1}{\sqrt{3}}(|e, g, g\rangle + |g, e, g\rangle - |e, e, g\rangle)$. Thus the group A_j can be seen as a “giant” atom effectively with only two levels $|g\rangle^{\otimes n_j}$ and $|s\rangle$. The reason why $|s\rangle$ is superradiant can be seen by noticing the dipole-dipole interac-

tion (in the non-Hermitian representation) characterized by the decay terms $\sum_{ii'} \gamma_{ii'} \sigma_i^+ \sigma_{i'}^- \rightarrow \sum_{A_j} n_j \gamma_0 S_j^+ S_j^- + \sum_{A_j, A_{j'}} \sqrt{n_j n_{j'}} \gamma_0 S_j^+ S_{j'}^-$, where the first terms correspond to superradiant decay of A_j , and the second terms correspond to mutual decay channels between different giant atoms A_j and $A_{j'}$. There are no mutual decay terms between A_j and $B_{j'}$, and between B_j and $B_{j'}$. Similarly, the dipole-dipole interaction characterized by exchange $\sum_{ij} \Delta_{ij} \sigma_i^+ \sigma_j^- \rightarrow \sum_{A_j, B_{j'}, j < j'} \sqrt{n_j n_{j'}} \gamma_0 S_j^+ S_{j'}^-$. We can also treat $B_{j'}$ as a giant two-level atom in the same manner, we find the exchange coupling only exists between A_j and $B_{j'}$ when $j < j'$. For $j > j'$, from Eq. (4) where $\Delta_{ii'} \sim \sin k_0(x_i + x_{i'}) + \sin k_0|x_i - x_{i'}|$, the two sine terms differ by a phase of π and hence cancel out. This leads us to an effective reduced scheme represented by Fig. 6 (b), which will yield the same spectral behavior as the original one.

In the case of an array consisting of two groups A_1 and B_2 , with n_1 antinode and n_2 node qubits, respectively, it can be directly replaced by one antinode atom of linewidths $\sqrt{n_1} \gamma_0$ coupled to a node atom with exchange coupling $\sqrt{n_1 n_2} \gamma_0$. Thus, the CLS splitting is $\delta_{split} = 2\sqrt{n_1 n_2} \gamma_0$ without dephasing. Fig. 7 (a) presents the scaling law of δ_{split} , which indeed agrees with our prediction. Small deviation is visible but negligible when dephasing is included, and gradually vanishes as N gets large. In Fig. 7 (b) we compare the reflection spectral profile of two situations: $(x_1, x_2, x_3, x_4) = (0, 1, 2, 2.25)\lambda$ and $(0, 0.25, 0.75, 1.25)\lambda$. In both cases the splitting is the same $2\sqrt{3} \gamma_0$. But the former has a broadened linewidth $\sqrt{3} \gamma_0$ due to superradiant enhancement in A_1 .

V. CONCLUSION

In summary, we have studied the dipole-dipole interaction between artificial atoms mediated by 1D vacuum modes in a waveguide. Setting one end of the waveguide to be a mirror, we are allowed to probe the collective Lamb shift by studying the reflection spectrum. When an qubit is placed at the node, we isolate it from coupling to other qubits through real photon field. Instead, the exchange interaction via virtual photons remains at work, causing the collective Lamb splitting between symmetric and antisymmetric levels that can now be clearly visible by means of a very simple reflection measurement. Our calculation highly agrees with the experimental results in [34]. We have derived the master equation to describe general cases and given analytical expressions for certain circumstances. We have also investigated the effects of dephasing, and the scaling law when more qubits are added. For special cases with many qubits placed only at antinodes and nodes, we have developed a reduced scheme under the weak field approximation, and explained the scaling behavior. For future outlook, we find close connection of our findings to a recent work [50], where atoms are considered large compared to the tran-

sition wavelength, and thought to have multiple chances of interaction before the field leaves. We expect similar analysis for some interesting interference effects, and our results can be very useful for quantum optical study and quantum simulation.

ACKNOWLEDGMENTS

K.-T. L. acknowledges Zih-Sin Chan and Yun-Chih Liao for helpful discussion. I.-C. H. acknowledges financial support from the MOST of Taiwan under Grant No. 107-2112-M-007-008-MY3. G.-D. L. acknowledges Anton Frisk Kockum for helpful feedback, and also the support from the MOST of Taiwan under Grant No. 105-2112-M-002-015-MY3 and National Taiwan University under Grant No. NTUCC-108L893206.

APPENDIX

A. Derivation of dipole-dipole interaction

In this section, we give detailed derivation of the dipole-dipole interaction, Eqs. (3) and (4), in a 1D waveguide and the master equation (2) in the main text. According to the Hamiltonian (1), the equations of motion for the field operator a_ω and an arbitrary atomic observable Q of the system are given respectively by

$$\dot{a}_\omega = -i\omega a_\omega - \sum_{i=1}^N g_i(\omega) \cos(k_\omega x_i) \sigma_i^-(t) \quad (\text{A.1})$$

and

$$\begin{aligned} \dot{Q} = & -\frac{i}{\hbar} \sum_{i=1}^N [Q, H_s] \\ & + \sum_{i=1}^N \int d\omega g_i(\omega) \cos(k_\omega x_i) [Q, a_\omega \sigma_i^+] + H.c.. \end{aligned} \quad (\text{A.2})$$

Integrating Eq. (A.1), we obtain

$$\begin{aligned} a_\omega(t) = & a_\omega(0) e^{-i\omega t} \\ & - \int_0^t dt' e^{i\omega(t-t')} \sum_{i=1}^N g_i(\omega) \cos(k_\omega x_i) \sigma_i^-(t'), \end{aligned} \quad (\text{A.3})$$

which, under the weak coupling and Born-Markov approximation, becomes

$$a_\omega(t) = - \sum_{i=1}^N \frac{g_i(\omega) \cos(k_\omega x_i)}{\epsilon + i(\omega - \omega_i)} \sigma_i^-(t) + \xi_\omega. \quad (\text{A.4})$$

Here, we have used $\sigma_i^-(t') \approx \sigma_i^-(t) e^{i\omega_i(t-t')}$ and taken the upper limit of the integral $t \rightarrow \infty$. Also, the term

regarding $a_\omega(0)$ contributes to a noise operator averaged out in the vacuum state. Note that the insertion of a small positive quantity ϵ is to guarantee the convergence of the integration. Substituting Eq. (A.4) into Eq. (A.2), we get

$$\dot{Q} = -\frac{i}{\hbar} \sum_{i=1}^N [Q, H_s] - \sum_{i,j=1}^N F_{ij}(\omega, x) [Q, \sigma_i^+] \sigma_j^- + H.c. \quad (\text{A.5})$$

with

$$F_{ij}(\omega, x) = \int_0^\infty \frac{g_i(\omega) g_j(\omega) \cos(k_\omega x_i) \cos(k_\omega x_j)}{\epsilon + i(\omega - \omega_j)} d\omega \quad (\text{A.6})$$

accounting for the dipole-dipole interaction. Thus, the decay rates and energy shift correspond to the real and imaginary part of $F_{ij} \equiv \gamma_{ij} + i\Delta_{ij}$, respectively [38]. Using the technique of contour integration, we finally obtain

$$\gamma_{ij} = \frac{\gamma_{ij}^0}{2} [\cos k_j(x_i + x_j) + \cos k_j |x_i - x_j|] \quad (\text{A.7})$$

$$\Delta_{ij} = \frac{\gamma_{ij}^0}{2} [\sin k_j(x_i + x_j) + \sin k_j |x_i - x_j|] \quad (\text{A.8})$$

where $\gamma_{ij}^0 \equiv \pi g_i(\omega_j) g_j(\omega_j)$. Note that in the most general case with non-identical qubits, $\gamma_{ij}^0 \neq \gamma_{ji}^0$.

B. Multi-level system

This section summarizes the general form for multi-level atoms of the master equation and dipole-dipole interaction among transmon qubits in the setup of this work. When a collection of such atoms with states $\{|n\rangle_i\}$ ($i = 1, 2, \dots, N$ is the atom index; $n = 0, 1, \dots$ is the state index) pumped by a single-mode field, the interaction Hamiltonian can be described by

$$H_{int} = i\hbar \sum_{i,n} \sqrt{n} g_i(\omega) \cos \frac{\omega}{c} x_i [a_\omega \sigma_{n,n-1}^i - H.c.], \quad (\text{A.9})$$

where $\sigma_{n,m}^i \equiv |n\rangle_i \langle m|$ is the jumping operator taking the i th atom from state $|m\rangle_i$ to state $|n\rangle_i$. Through the standard procedure discussed in the previous section, we derive the master equation that reads

$$\begin{aligned} \frac{d\rho}{dt} = & i \sum_{i,n} [\delta_n^i |n\rangle_i \langle n|, \rho] \\ & + i \sum_{i,n} \sqrt{n} \Omega_p^i [\sigma_{n,n-1}^i + H.c., \rho] \\ & - i \sum_{i,j,m,n} \left\{ \frac{(\Delta_{ij,m} + \Delta_{ji,n}) - i(\gamma_{ij,m} - \gamma_{ji,n})}{2} \right\} \times \\ & \sqrt{nm} [\sigma_{n,n-1}^i \sigma_{m-1,m}^j, \rho] \\ & + \sum_{i,j,m,n} \left\{ \frac{(\gamma_{ij,m} + \gamma_{ji,n}) + i(\Delta_{ij,m} - \Delta_{ji,n})}{2} \right\} \times \\ & \sqrt{nm} \mathcal{L}_{n,n-1;m-1,m}^{ij} [\rho] \\ & + \sum_{i,n} \gamma_{i,n}^\phi D_{i,n} [\rho] \end{aligned} \quad (\text{A.10})$$

with the decay rates and energy shifts

$$\gamma_{ij,n} = \frac{\pi g_i(\omega_n^j) g_j(\omega_n^j)}{2} \times \left[\cos \frac{\omega_n^j}{c} (x_i + x_j) + \cos \frac{\omega_n^j}{c} |x_i - x_j| \right] \quad (\text{A.11})$$

$$\Delta_{ij,n} = \frac{\pi g_i(\omega_n^j) g_j(\omega_n^j)}{2} \times \left[\sin \frac{\omega_n^j}{c} (x_i + x_j) + \sin \frac{\omega_n^j}{c} |x_i - x_j| \right] \quad (\text{A.12})$$

respectively, associated with state $|n\rangle$. Also, the incoherent jumping and dephasing superoperators are $\mathcal{L}_{mn,m'n'}^{ij}[\rho]_{nm} = 2\sigma_{m'n'}^j \rho \sigma_{mn}^i - \rho \sigma_{mn}^i \sigma_{m'n'}^j - \sigma_{mn}^i \sigma_{m'n'}^j \rho$ and $D_{i,n}[\rho] = 2\sigma_{nn}^i \rho \sigma_{nn}^i - \rho \sigma_{nn}^i - \sigma_{nn}^i \rho$, respectively. By solving the master equation, one can obtain the reflection coefficient through

$$r = \left| 1 + i2 \frac{Q^N}{\Omega_{01}^N} \sum_{i,n} \frac{\gamma_{ii,n}}{Q^i} \sqrt{n} \cos k_p x_i \langle \sigma_{n-1,n}^i \rangle \right|, \quad (\text{A.13})$$

where $Q^n = \sqrt{2} e \beta_n (E_J^{(n)} / 8 E_c^{(n)})^{1/4}$.

-
- [1] W. E. Lamb and R. C. Retherford, Phys. Rev. **72**, 241 (1947).
 - [2] H. J. Carmichael, A. S. Lane, and D. F. Walls, Phys. Rev. Lett. **58**, 2539 (1987).
 - [3] S. Schiller, G. Breitenbach, S. F. Pereira, T. Müller, and J. Mlynek, Phys. Rev. Lett. **77**, 2933 (1996).

- [4] H. B. G. Casimir, Proc. Kon. Nederland. Akad. Wetensch. **B51**, 793 (1948).
- [5] M. Bordag, U. Mohideen, and V. Mostepanenko, Physics Reports **353**, 1 (2001).
- [6] C. M. Wilson, G. Johansson, A. Pourkabirian, M. Simoen, J. R. Johansson, T. Duty, F. Nori, and P. Delsing, Nature **479**, 376 (2011).

- [7] F. Le Kien, S. D. Gupta, K. P. Nayak, and K. Hakuta, Phys. Rev. A **72**, 063815 (2005).
- [8] B. Zhu, J. Cooper, J. Ye, and A. M. Rey, Phys. Rev. A **94**, 023612 (2016).
- [9] S. L. Bromley, B. Zhu, M. Bishof, X. Zhang, T. Bothwell, J. Schachenmayer, T. L. Nicholson, R. Kaiser, S. F. Yelin, M. D. Lukin, A. M. Rey, and J. Ye, Nature Communications **7**, 11039 (2016).
- [10] E. Shahmoon, D. S. Wild, M. D. Lukin, and S. F. Yelin, Phys. Rev. Lett. **118**, 113601 (2017).
- [11] J. Perczel, J. Borregaard, D. E. Chang, H. Pichler, S. F. Yelin, P. Zoller, and M. D. Lukin, Phys. Rev. Lett. **119**, 023603 (2017).
- [12] I. I. Beterov, G. N. Khamzina, D. B. Tret'yakov, V. M. Entin, E. A. Yakshina, and I. I. Ryabtsev, Quantum Electronics **48**, 453 (2018).
- [13] F. Arecchi and D. Kim, Optics Communications **2**, 324 (1970).
- [14] R. Friedberg, S. Hartmann, and J. Manassah, Physics Reports **7**, 101 (1973).
- [15] M. O. Scully, Phys. Rev. Lett. **102**, 143601 (2009).
- [16] M. O. Araújo, I. Krešić, R. Kaiser, and W. Guerin, Phys. Rev. Lett. **117**, 073002 (2016).
- [17] S. J. Roof, K. J. Kemp, M. D. Havey, and I. M. Sokolov, Phys. Rev. Lett. **117**, 073003 (2016).
- [18] J. Keaveney, A. Sargsyan, U. Krohn, I. G. Hughes, D. Sarkisyan, and C. S. Adams, Phys. Rev. Lett. **108**, 173601 (2012).
- [19] T. Peyrot, Y. R. P. Sortais, A. Browaeys, A. Sargsyan, D. Sarkisyan, J. Keaveney, I. G. Hughes, and C. S. Adams, Phys. Rev. Lett. **120**, 243401 (2018).
- [20] R. Röhlsberger, K. Schlage, B. Sahoo, S. Couet, and R. Ruffer, Science **328**, 1248 (2010).
- [21] Z. Meir, O. Schwartz, E. Shahmoon, D. Oron, and R. Ozeri, Phys. Rev. Lett. **113**, 193002 (2014).
- [22] X. Gu, A. F. Kockum, A. Miranowicz, Y.-x. Liu, and F. Nori, Physics Reports **718-719**, 1 (2017).
- [23] J. M. Fink, R. Bianchetti, M. Baur, M. Göppl, L. Steffen, S. Filipp, P. J. Leek, A. Blais, and A. Wallraff, Phys. Rev. Lett. **103**, 083601 (2009).
- [24] S. Filipp, M. Göppl, J. M. Fink, M. Baur, R. Bianchetti, L. Steffen, and A. Wallraff, Phys. Rev. A **83**, 063827 (2011).
- [25] K. Lalumière, B. C. Sanders, A. F. van Loo, A. Fedorov, A. Wallraff, and A. Blais, Phys. Rev. A **88**, 043806 (2013).
- [26] A. F. van Loo, A. Fedorov, K. Lalumière, B. C. Sanders, A. Blais, and A. Wallraff, Science **342**, 1494 (2013).
- [27] J. A. Mlynek, A. A. Abdumalikov, C. Eichler, and A. Wallraff, Nature Communications **5**, 5186 (2014).
- [28] M. Mirhosseini, E. Kim, X. Zhang, A. Sipahigil, P. B. Dieterle, A. J. Keller, A. Asenjo-Garcia, D. E. Chang, and O. Painter, arXiv:1809.09752 (2018).
- [29] N. Lambert, Y. Matsuzaki, K. Kakuyanagi, N. Ishida, S. Saito, and F. Nori, Phys. Rev. B **94**, 224510 (2016).
- [30] P. Facchi, M. S. Kim, S. Pascazio, F. V. Pepe, D. Pomarico, and T. Tufarelli, Phys. Rev. A **94**, 043839 (2016).
- [31] Z. Liao and M. S. Zubairy, Phys. Rev. A **98**, 023815 (2018).
- [32] I.-C. Hoi, A. F. Kockum, L. Tornberg, A. Pourkabirian, G. Johansson, P. Delsing, and C. M. Wilson, Nature Physics **11**, 1045 (2015).
- [33] P. Y. Wen, A. F. Kockum, H. Ian, J. C. Chen, F. Nori, and I.-C. Hoi, Phys. Rev. Lett. **120**, 063603 (2018).
- [34] P. Y. Wen, K.-T. Lin, A. F. Kockum, B. Suri, H. Ian, J. C. Chen, S. Y. Mao, C. C. Chiu, P. Delsing, F. Nori, G.-D. Lin, and I.-C. Hoi, (2019), arXiv:1904.12473.
- [35] J. Koch, T. M. Yu, J. Gambetta, A. A. Houck, D. I. Schuster, J. Majer, A. Blais, M. H. Devoret, S. M. Girvin, and R. J. Schoelkopf, Phys. Rev. A **76**, 042319 (2007).
- [36] B. Peropadre, J. Lindkvist, I.-C. Hoi, C. M. Wilson, J. J. Garcia-Ripoll, P. Delsing, and G. Johansson, New Journal of Physics **15**, 035009 (2013).
- [37] U. Dörner and P. Zoller, Phys. Rev. A **66**, 023816 (2002).
- [38] R. H. Lehmberg, Phys. Rev. A **2**, 883 (1970).
- [39] H. T. Dung, L. Knöll, and D.-G. Welsch, Phys. Rev. A **66**, 063810 (2002).
- [40] K. Koshino and Y. Nakamura, New Journal of Physics **14**, 043005 (2012).
- [41] B. Yurke and J. S. Denker, Phys. Rev. A **29**, 1419 (1984).
- [42] H. J. Carmichael, *Statistical Methods in Quantum Optics 1: Master Equations and Fokker-Planck Equations (Theoretical and Mathematical Physics) (v. 1)* (Springer, 2003).
- [43] M. O. Scully, *Quantum Optics* (Cambridge University Press, 1997).
- [44] J. Q. You and F. Nori, Nature **474**, 589 (2011).
- [45] J. M. M. H. Devoret, A. Wallraff, arXiv:cond-mat/0411174 (2004).
- [46] D. Chang, L. Jiang, A. V. Gorshkov, and H. J. Kimble, New Journal of Physics **14**, 063003 (2012).
- [47] P. Solano, P. Barberis-Blostein, F. K. Fatemi, L. A. Orozco, and S. L. Rolston, Nature Communications **8**, 1857 (2017).
- [48] W. Guerin and R. Kaiser, Phys. Rev. A **95**, 053865 (2017).
- [49] A. Blais, R.-S. Huang, A. Wallraff, S. M. Girvin, and R. J. Schoelkopf, Phys. Rev. A **69**, 062320 (2004).
- [50] A. F. Kockum, G. Johansson, and F. Nori, Phys. Rev. Lett. **120**, 140404 (2018).